Deformation and failure mechanism of dynamically loaded sandwich beams with aluminum-foam core [☆]

J.L. Yu*, X. Wang, Z.G. Wei, E.H. Wang

Key Laboratory of Mechanical Behavior and Design of Materials, University of Science and Technology of China, CAS, Hefei, Anhui 230026, People's Republic of China

Abstract

In this paper the response and failure of dynamically loaded sandwich beams with an aluminum-foam core is investigated experimentally. The dynamic compressive stress–strain curves of the core material, an open-cell aluminum foam, are obtained by an SHPB technique. No strain-rate sensitivity is found. Quasi-static and dynamic bending tests are carried out for sandwich beams made of aluminum skins with an aluminum foam core. The deformation and failure mechanism are revealed by 'frozen' test using stop blocks. It is found that due to large local indentation and damage the energy absorbing capacity of beams loaded dynamically is lower than that for quasi-static loading.
© 2002 Elsevier Science Ltd. All rights reserved.

Keywords: Aluminum foam; Foam core sandwich beams; Dynamic response; Impact failure; Energy absorption

1. Introduction

In the last two decades metallic foams have been developed and are growing in use as new engineering materials. These ultra-light metal materials possess unique mechanical properties, such as high rigidity and high impact energy absorption at low weight, equal properties in all directions giving tolerance to varying direction of loading, stable deformation mode and adaptation to loading condition during deformation, etc. Potential applications include energy absorbers in the automotive industry and other equipment for transportation, packaging (protection from shock for heavy components that are sensitive to impact), core material in

sandwich structures with special requirements, and core material in hollow structures to prevent buckling.

1.1. Quasi-static mechanical behavior

When a block of foam is compressed, the stress–strain curve shows three regions. At low strains, the foam deforms in a linear-elastic way, then a plateau of deformation at almost constant stress occurs, and finally there is a region of densification as the cell walls crush together. The extent of each region depends on the relative density ρ/ρ_s. Elastic foams, plastic foams, and even brittle foams all have generalized three-part stress–strain curves like this, though the mechanism is different in each case.

The Young's modulus and compressive strength of metallic foams have been measured by a number of researchers [1–4]. However, most commercially available cellular metals, unlike some of their polymer counterparts, do not achieve the properties predicted by theoretical models according to the properties of the cell wall material and the relative density of the foam [5]. Various hypotheses have been made regarding the 'defect' that diminishes the properties [6–8].

1.2. Dynamic mechanical behavior

In order to evaluate the capacity of impact energy absorption, the strain-rate sensitivity of the foam material must be characterized. The SHPB method has been used for measuring the dynamic compressive response of cellular materials, including polymers and metals.

Only limited data are available for the strain-rate dependence of the compression strength of cellular materials. Lankford and Dannemann [9] reported that the strain-rate dependence was negligible for a low-density open-cell 6101 Al foam. Recently, Deshpande and Fleck [10] investigated the high-strain-rate compressive behavior of the closed cell aluminum alloy foam Alulight and the open cell aluminum alloy foam Duocel for strain rates up to $5000 \, s^{-1}$ using SHPB and direct impact tests. It was found that the dynamic behavior of these foams was very similar to their quasi-static behavior. On the other hand, Mukai et al. [11,12] and Kanahashi et al. [13] reported that an open cell magnesium foam AZ91, an open cell aluminum foam SG91A and a closed cell aluminum foam ALPORAS all exhibited high-strain-rate sensitivity of the plateau stress. They also found that the absorption energy normalized by the relative density at dynamic strain rates was about 60% higher than that at quasi-static strain rates. Paul and Ramamurty [14] investigated the strain-rate sensitivity of a closed cell aluminum foam under nominal strain rates from 3.33×10^{-5} to $1.6 \times 10^{-1} \, s^{-1}$. Within this range, they found that the plastic strength and the energy absorbed increased by 31 and 52.5%, respectively, with increasing strain rate.

1.3. Foam core structures

Metal foams are frequently used in the form of foam core structures. In engineering applications, energy-absorbing structures work at the post-failure stage; some sandwich structures must be capable of sustaining large overload, e.g. foreign-object impact. In these cases, the non-linear (failure) behavior of the structure is important and the parameters of interest are the

load-carrying capacity, the integrity of the structure and the energy-absorbing capabilities of the structure before total collapse.

The study in this area mainly begins in the recent few years. Chen et al. [15] and Bart-Smith et al. [16] investigated quasi-static failure modes of sandwich beams with aluminum foam core in bending. They found three collapse modes: face yield, indentation and core shear. Failure maps based on analytical models were presented. McCormack et al. [17] pointed face wrinkle as an additional failure mode but they found experimentally that core shear and indentation were the dominant failure modes. Kesler and Gibson [18] studied the size effect of foam shear strength on the limited load of foam core sandwich beams. Harte et al. [19] investigated the fatigue strength and failure modes of sandwich beams. They also explored the failure modes of aluminum skin-Alporas foam core sandwich panels and constructed maps dependent on the sandwich panel geometry [20]. In all these investigations, only quasi-static loading was considered.

Hanssen et al. [21,22] investigated static and dynamic crushing of square and circular aluminum extrusions with aluminum foam filler. Santosa and Wierzbicki [23] and Santosa et al. [24] studied the planar bending response of thin-walled beams with low-density metal filler and found that the bending resistance was improved dramatically by aluminum foam filler. The presence of the foam filler changes the crushing mode of the thin-walled beam and prevents the drop in load-carrying capacity. This was also observed by Hanssen et al. [25] who carried out static three-point-bending tests of square aluminum extrusions with aluminum foam filler. Design formulas were suggested for prediction of the initial peak load, the load after tensile failure of the foam core, and the ultimate capacity.

In the present paper, the responses of an open-cell aluminum foam and aluminum skin–aluminum foam core beams under dynamic compression and bending, respectively, are investigated and the deformation and failure mechanism are compared with the quasi-static behavior. It is found that the foam tested exhibits no strain-rate sensitivity. Under impact loading the upper skin of the sandwich beams wrinkles first, accompanied with local debonding between the upper skin and the core. The final failure occurs when the lower skin is broken. This is similar to one of the failure modes found under quasi-static loading.

2. Dynamic compression of aluminum foam

2.1. Material and specimens

An open-cell aluminum foam was used in experiments. The material was provided by the Institute of Solid Physics, Chinese Academy of Sciences. The relative density of the aluminum foam is 0.37 and the average cell size is 1.5 mm. The components of the cell wall material are listed in Table 1. This material was made by grain-casting method. In this method, melted liquid metal is

Table 1
The components of the cell wall material

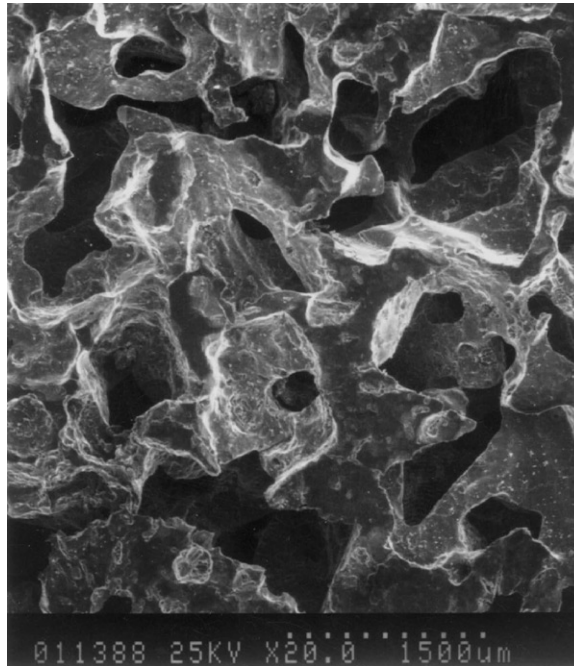| Component	Al	Si	Fe	Cu	Impurity
Content (%)	⩾98	⩽1.8	⩽1	⩽0.05	⩽2.0

Fig. 1. SEM photograph of the undeformed alumunium foam material.

first poured into a bed of leachable particles and then, after concretion of the metal, the particles are dissolved. So the shape and size of cells depend on the particles. In our case, the meso-structure of the foam differs much from the ideal foam structure. The density is relatively high and the topology of the foam is not the same as the Gibbs–Ashby model. The SEM photograph of undeformed aluminum foam material is given in Fig. 1. Unlike slender edges in regular open cell foam, anomalous sheet edges were found.

Cylindrical specimens 30 mm in diameter were used, which were cut from a block using an EDM (electric discharge machine). Two different values of thickness, 10 and 20 mm, were used in the tests.

2.2. Experimental results

Dynamic compression tests were preformed using a split Hopkinson pressure bar. No significant difference in the dynamic response between specimens of 10 mm thickness and those of 20 mm thickness was found. The dynamic response agrees well with the quasi-static response. A comparison of quasi-static ($\dot{\varepsilon} = 10^{-3} \, \text{s}^{-1}$) and dynamic ($\dot{\varepsilon} = 1000 \sim 1750 \, \text{s}^{-1}$) nominal stress–strain curves of the aluminum foam specimens is shown in Fig. 2. It is obvious that there is no consistent trend with increasing strain rate. So, the foam material studied is strain-rate-insensitive.

Fig. 3 gives the SEM photographs of dynamically compressed specimens. There is evidence that the aluminum foam is crushed in a spatially uniform manner both at quasi-static rate and in the
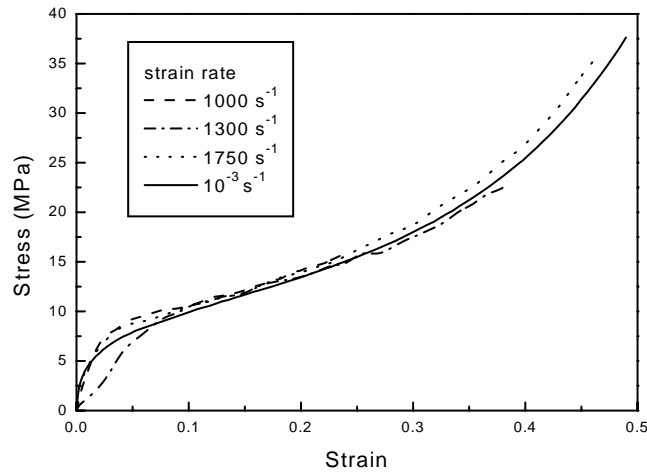
Fig. 2. Comparison of the quasi-static and dynamic stress–strain curves of the aluminum foam under compression.
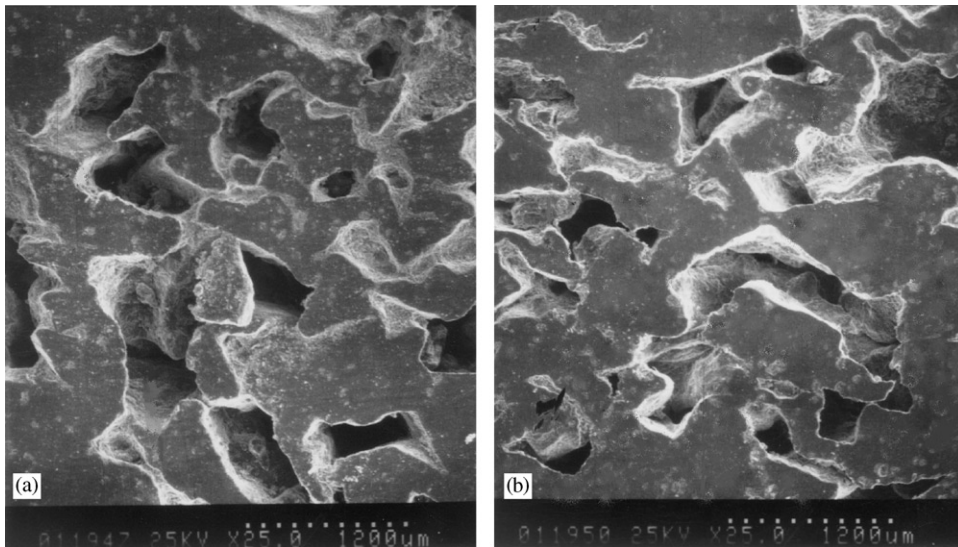

Fig. 3. Mid-plane SEM photographs of dynamically deformed open-cell aluminum foam specimens: (a) $\varepsilon = 0.18$ and (b) $\varepsilon = 0.26$.

dynamic split Hopkinson bar tests. It indicates that the foam deformation is uniform with no crush band formation. This is likely due to the anomalous sheet-edge structure mentioned before. We conclude that, for the foam tested, the mode of dynamic collapse ($\dot{\varepsilon} < 1800 \, \mathrm{s}^{-1}$) is qualitatively the same as that under quasi-static loading. For comparison, in their SHPB tests, Deshpande and Fleck [10] reported that open-cell Duocel foam specimens deformed uniformly while the closed-cell Alulight foam specimens did not.

3. Static and dynamic tests of aluminum form core sandwich beams

3.1. Experiments and results

Sandwich beams were made up of two thin skins adhered to an open cell aluminum foam core by a commercially available acrylate adhesive. The skin material was aluminum $L5Y_2$ (Chinese shop sign, equivalent to 1100 aluminum in US). The thickness of the aluminum skin was 0.5 mm. The engineering tensile stress–strain curves are shown in Fig. 4, which were measured using the same sheet. The core material was the same as that used in the compression tests. Three different values of nominal core thickness, i.e. 10, 15 and 20 mm, were chosen. The length of the beam specimens was 300 mm. Drawing of the sandwich beams is shown in Fig. 5.

Static tests were conducted on an MTS810 testing system using a three-point bending rig at a crosshead speed of 0.025 mm/s. The specimen was put on two steel cylinders of 10 mm in diameter with a span of 250 mm. The head of the loading device is shown in Fig. 6.

Table 2 gives the details of the tests, where c is the core thickness, B the beam width, I the initial bending stiffness, D the total energy absorbed. P_u and δ_b are respectively the maximum force and
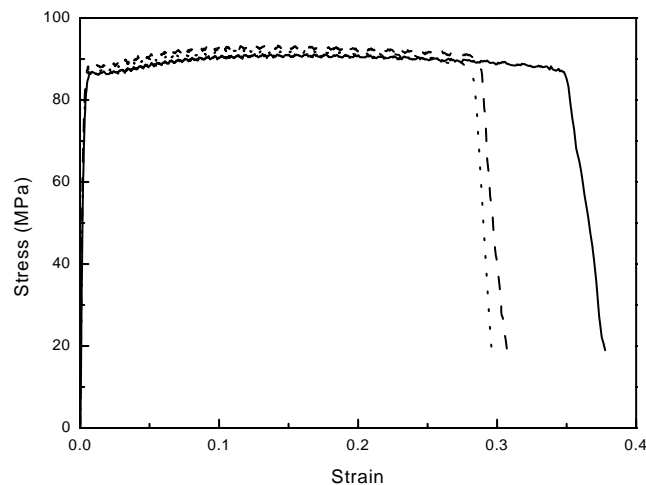

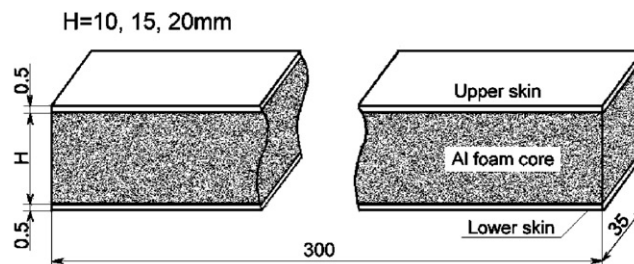Fig. 4. Engineering stress–strain curves of the aluminum skin.
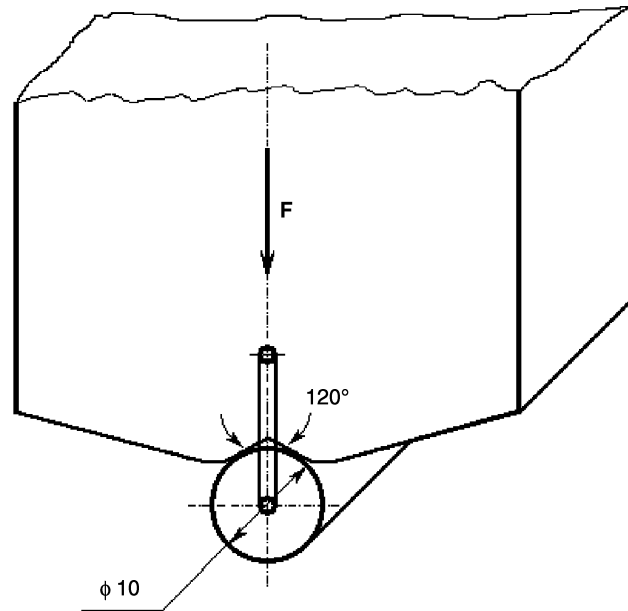

Fig. 5. Drawing of the sandwich specimen.

Fig. 6. Head of the loading device in static bending tests.

Table 2
Details of the quasi-static three-point bending tests

Specimen number	c (mm)	B (mm)	I (N m^2)	Failure mode	P_u (kN)	δ_b (mm)	D (J)
A10-1	9.60	35.25	72.31	I	0.46	16.1	8.78
A10-2	9.57	35.03	44.43	II	0.39	22.9	9.74
A10-3	9.51	34.99	61.91	II	0.43	22.9	10.82
A15-1	16.74	34.81	140.53	I	0.58	11.3	8.41
A15-2	15.85	35.07	137.36	II	0.45	20.9	12.05
A15-3	15.83	34.79	139.26	I	0.64	13.3	10.20
A15-4	15.74	35.00	95.821	II	0.50	26.1	14.78
A20-1	20.10	35.19	203.92	I	0.79	9.9	10.10
A20-2	20.31	34.87	199.25	II	0.65	17.1	13.10

the deflection when the beam breaks off. The measured load-deflection curves of the static three-point bending of the sandwich beams with different core thickness are given in Fig. 7.

Impact tests were conducted on a drop weight machine. The mass of the hammer was 2.58 kg and the drop height was 0.8 m. This holds an initial impact energy of about 20 J. In order to get information of the deformation and failure process, different 'stop blocks' were used to limit the final deflection δ. The support condition was the same as that in the static tests. A photograph of the specimen and the hammer with 'stop-blocks' after a test is shown in Fig. 8. A complete drawing of the hammer is shown in Fig. 9. It should be noted that the radius of the loading head is
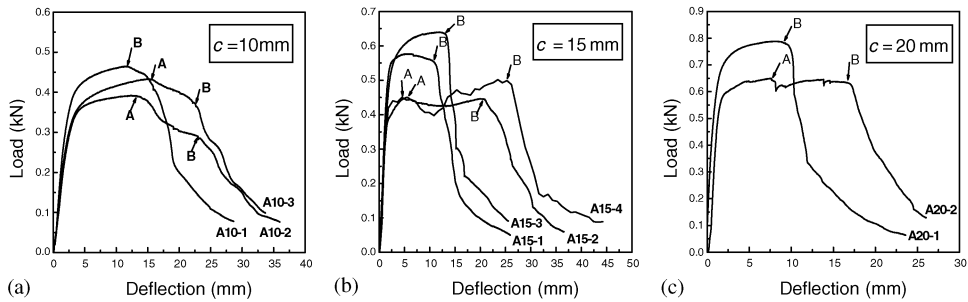
Fig. 7. Load-deflection curves of the sandwich beams: (A) load drop due to upper skin wrinkling; (B) initiation of lower skin failure.
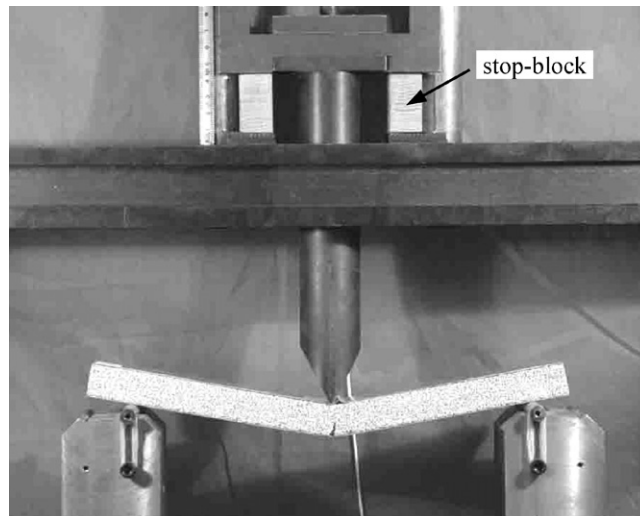

Fig. 8. Photograph of the specimen and the hammer with 'stop-blocks' after a test.

2.5 mm, smaller than that in quasi-static tests (5 mm). An accelerometer was embedded inside the hammer in order to get the velocity and displacement history. In some tests, a CCD type high-speed camera SPEEDCAM PRO-LT was used to record the change of the specimen profile during the test with a frame rate of 1000 fps. A typical photo is shown in Fig. 10. Rebound and repeated impact of the hammer on the beams were found from the high-speed camera record. However, no further increase in deflection occurred after the first impact.

Permanent transverse profiles of the sandwich beams after impact are shown in Fig. 11. Details of the impact tests are given in Table 3, where δ_I, δ_M and δ_f are the maximum displacement of the hammer after the first impact calculated by integration of the accelerometer signal, the maximum deflection after the first impact obtained from the high-speed camera record, and the permanent deflection measured after test, respectively. It should be noted that δ_M would normally exceed δ_I due to the inertia effect of the beam, while δ_f should be less than δ_M because of elastic recovery.
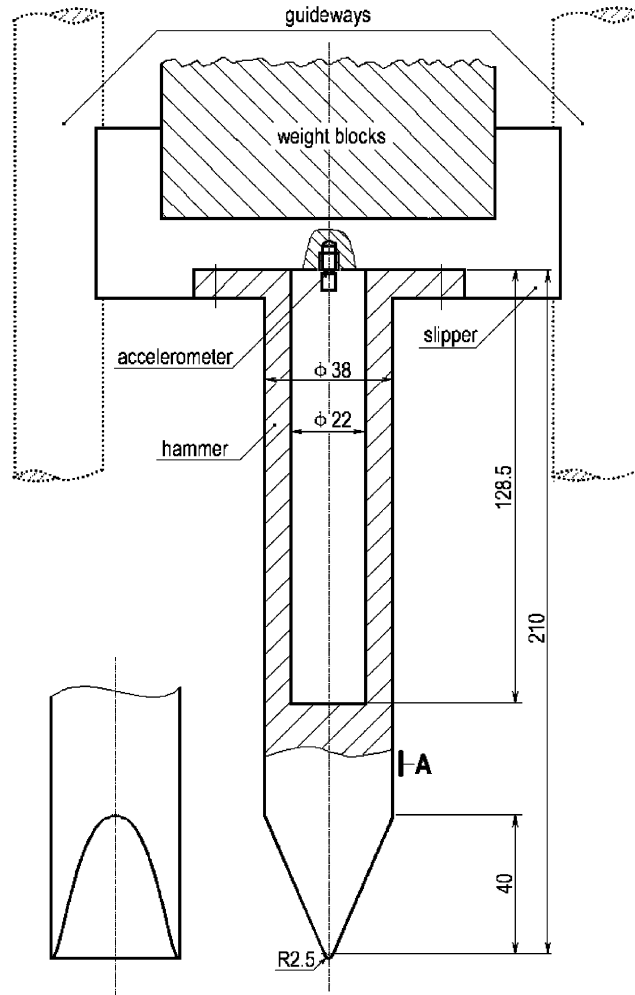
Fig. 9. Complete drawing of the hammer.

A typical record of the accelerometer is shown in Fig. 12. The large deceleration after 6 ms shown in the figure is due to the impact of the hammer with the stop block. The histories of the hammer velocity and displacement are then obtained by integration of the accelerometer signal. The displacement is identical with the beam deflection before separation of hammer and beam. The velocity vs. time curves of the hammer for beams with nominal core thickness of 10 and 15 mm are shown in Figs. 13a and b, respectively. These figures together with the data of δ_I, δ_M and δ_f listed in Table 3, to some extent, reflect the repeatability and accuracy of the dynamic tests. In considering the unstable nature of the local damage, the agreement is acceptable. The hammer velocity and displacement of three tests with different nominal thickness, for which final failure occurs, are shown in Figs. 14 and 15, respectively.
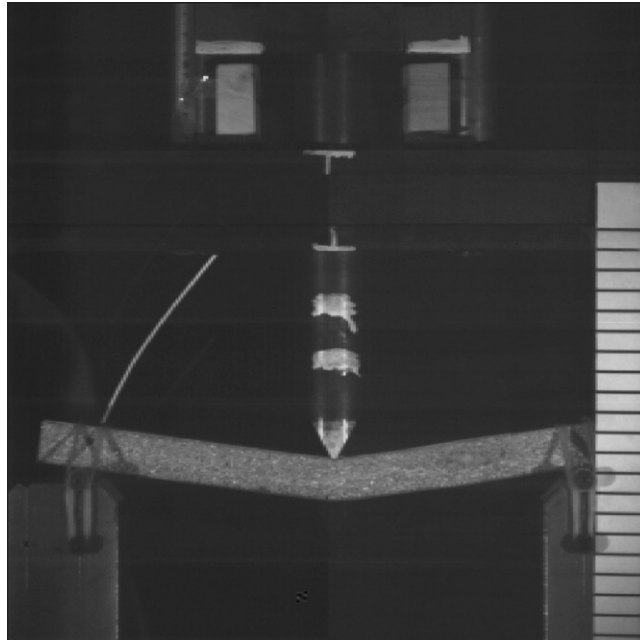
Fig. 10. Typical record of the high-speed camera.

It should be noted that the negative signal of deceleration in Fig. 12 is due to stress-wave effects, for the accelerometer is located about 21 cm from the impact point and attached on a surface inside the hammer, Fig. 9. Hence the accelerometer signal is related to the deceleration of the mass only in the average sense. Fourier transform reveals that the frequency of interferential signal is above 2500 Hz.

In considering the stress-wave effect mentioned above, the impact force could not be directly obtained from the accelerometer recording by multiplying with the mass. Rather, a multipoint-average-smoothing method is applied to the velocity history to reduce the 'noise'. 85-point average is chosen which corresponds to a characteristic time of 0.425 ms. Approximate force history is then obtained by differentiation of the smoothed velocity signal. Fig. 16 shows the smoothed velocity curve for specimen B15-3 by this way, in comparison with the original velocity signal. The dynamic force–deflection curve of specimen B15-3 so obtained is compared with the corresponding quasi-static tests, specimen A15-2 and A15-4, in Fig. 17. It is not surprising that an initial peak force occurs due to the inertia effect. However, the value of the initial peak is not credible because of the wave effect mentioned above. Nevertheless, the plateau does reflect the load capacity in the later stage.

It can be seen from Fig. 17 that the deflection at failure in the dynamic bending was significantly less than that in the quasi-static cases, presumably due to the relatively heavier local deformation and damage near the impact region in the dynamic case. On the other hand, aluminum is strain-rate-sensitive. So the skin is stronger in dynamic tests. In addition, inertia effect will further increase the reacting force. So the load-carrying capacity in dynamic case was higher than that in static cases. Even so, the energy-absorbing capacity in dynamic cases was reduced.
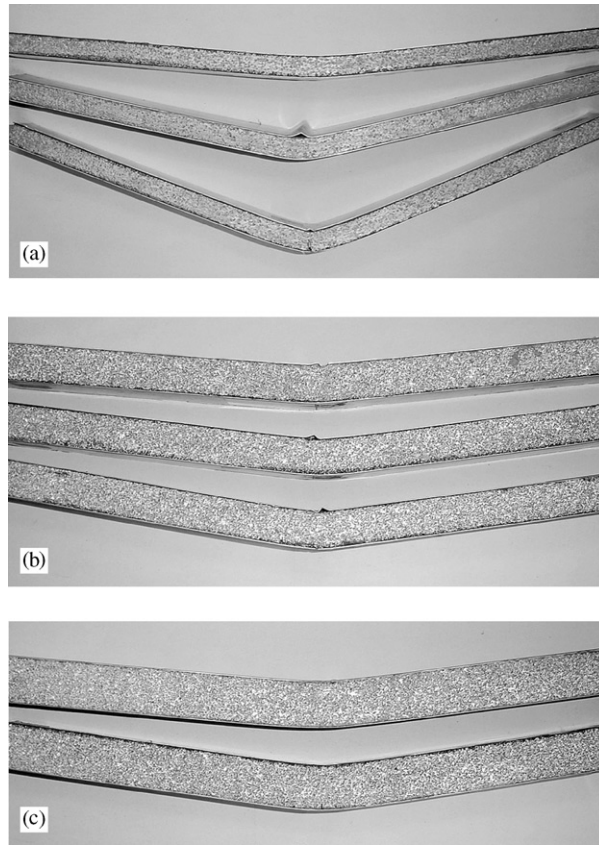
Fig. 11. Permanent transverse profiles of the sandwich beams after impact: (a) $c = 10$ mm; (b) $c = 15$ mm; (c) $c = 20$ mm.

Table 3
Details of the impact three-point bending tests

Specimen number	c (mm)	B (mm)	δ_I (mm)	δ_M (mm)	δ_f (mm)	Lower skin failure
B10-1	9.86	34.96	14.1	—	10.9	No
B10-2	9.64	35.28	28.6	28.8	26.0	No
B10-3	9.84	34.90	-	—	46.4	Yes
B15-1	16.50	34.90	12.9	—	10.6	No
B15-2	16.02	34.72	17.0	—	15.3	No
B15-3	16.20	35.00	20.8	—	18.6	Yes
B20-1	20.30	35.10	15.2	15.0	12.5	No
B20-2	20.22	35.72	18.1	18.7	17.0	Yes

Note: δ_I for specimen B10-3 is not available due to inadequate signal record.
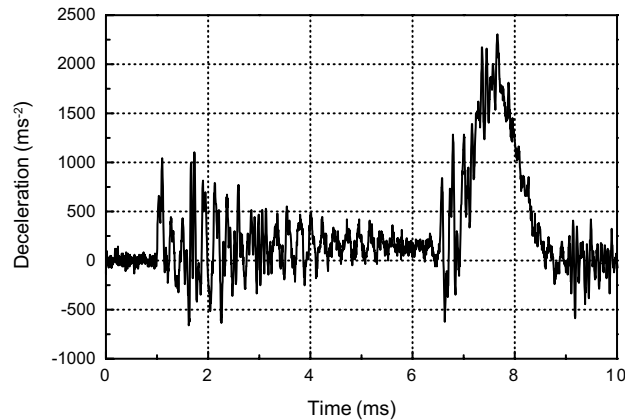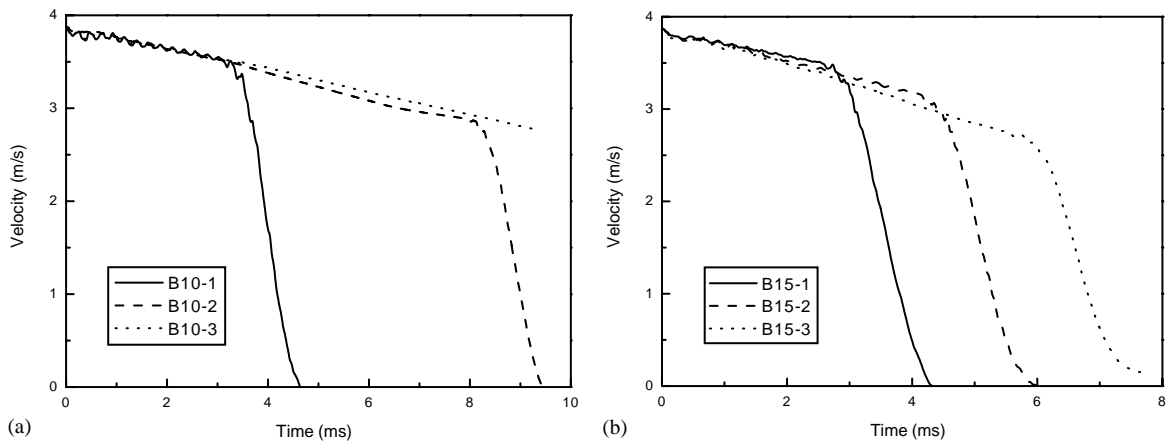
Fig. 12. Typical accelerometer record.

Fig. 13. Velocity vs. time curves of the hammer for beams with nominal core thickness of (a) 10 mm and (b) 15 mm.

3.2. Failure mechanism

Beams under quasi-static bending finally failed by tensile failure of the lower skin. Two failure modes can be distinguished. Mode I is without a wrinkle of the upper skin while Mode II has a wrinkle of the upper skin, as shown in Fig. 18. In both modes, the upper part of the core was compressed under the indentation, while a tensile crack was found in the lower part of the core. However, the associated load–deflection curves exhibit different characteristics. For Mode I failure, the maximum load is higher but the tensile failure of the lower skin occurs earlier. For Mode II failure, on the other hand, the beam can bear a lower, nearly constant load with a larger deflection at failure and thus absorbs more energy. This phenomenon is more distinct for thicker beams. Only a small wrinkle was found for specimens A10-2 and A10-3. The maximum load
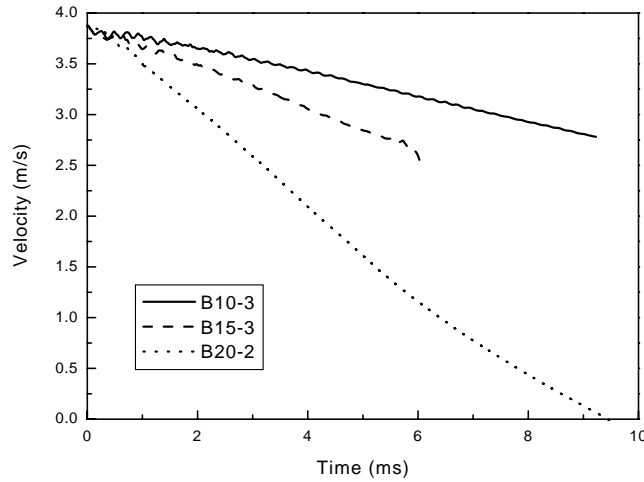
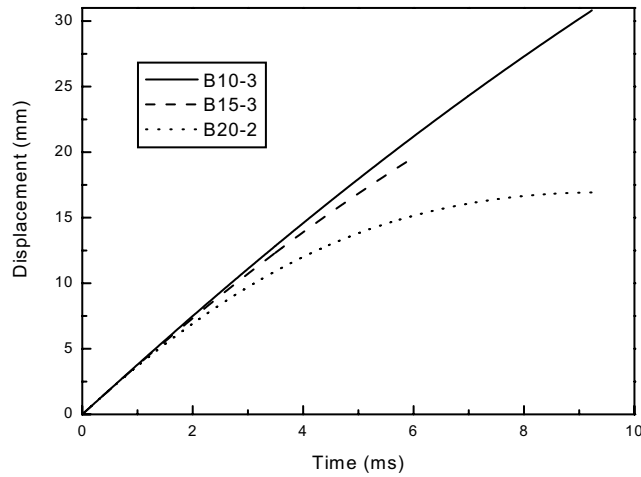Fig. 14. Velocity vs. time curves of the hammer for beams with different thicknesses.

Fig. 15. Displacement histories of the hammer for beams with different thicknesses.

increases with the thickness but thin beams can also absorb large energy because of the large deflection, as can be seen in Table 2 and Fig. 7.

In the present experiments, we did not find the core shear mode, which were reported in Refs. [15–17] for three-point or four-point bending of sandwich beams. This does not mean that core shear could not happen. Rather, it depends on the material property and specimen geometry. Nevertheless, a wrinkle of the upper skin in Mode II failure will significantly reduce the shear stress and the trend of shear failure.

The failure process of beams under impact loading can be revealed from a set of tests with different final deflections. The side views of specimens B15-1, B15-2 and B15-3 near the impact point are shown in Fig. 19. It can be seen from these pictures that, when a sandwich beam was
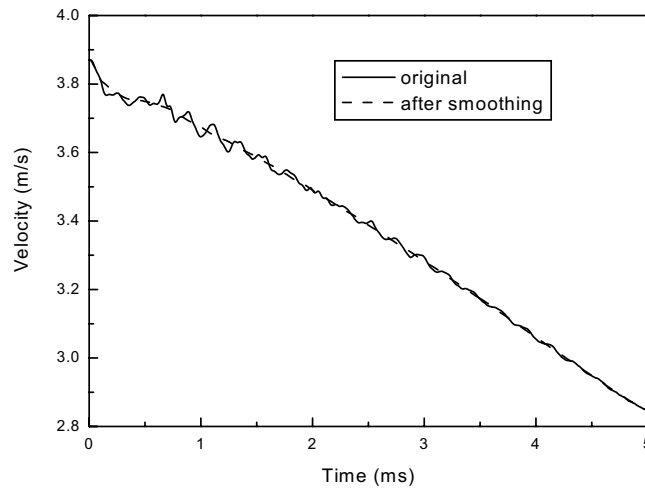
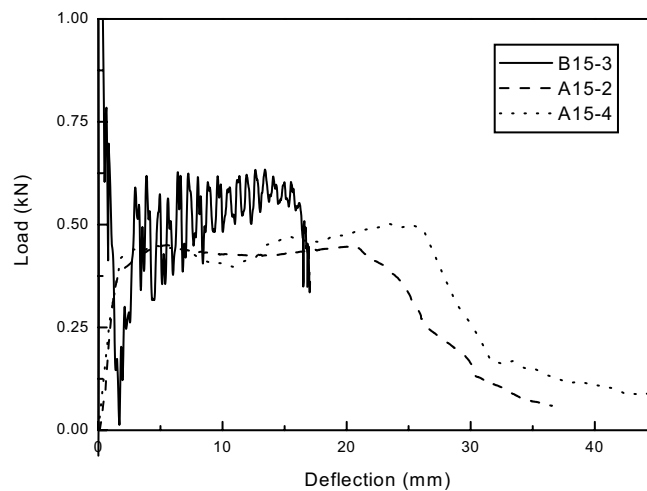Fig. 16. Comparison of the original and smoothed velocity profiles.

Fig. 17. Comparison of the quasi-static and dynamic force–deflection curves. The maximum load for B15-3 is 2.26 kN, not shown in the figure.

impacted by a mass, a wrinkle would first form near the impact point of the upper skin. This phenomenon was accompanied with local debonding between the upper skin and the core, as well as the compression of the upper core and tension of the lower core, Fig. 19a. Then a local stable squash may take place in the upper core, Fig. 19b. The final failure was the tensile failure of the lower core and lower skin, Fig. 19c. This failure mode is similar to Mode II of the quasi-static beam tests.

The fracture surfaces of the foam core in the ruptured beam specimens are examined using a scanning electron microscope. Both quasi-statically and dynamically loaded specimens show a
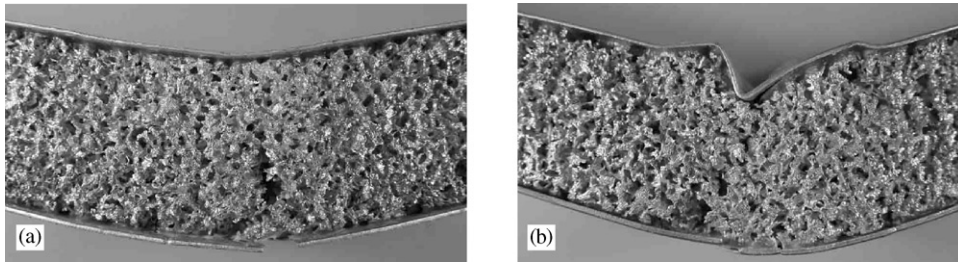
Fig. 18. Failure modes of beams under static bending: (a) failure Mode I (specimen A15-3), (b) failure Mode II (specimen A15-2).
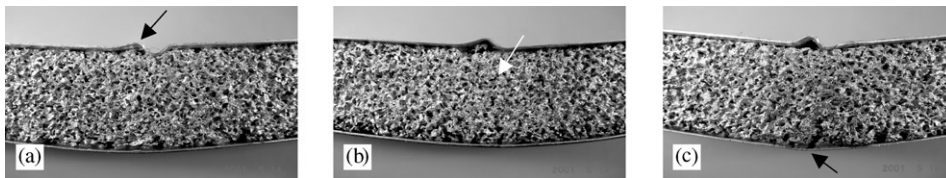

Fig. 19. Side view of specimens (a) B15-1 ($\delta = 12$ mm), (b) B15-2 ($\delta = 15$ mm) and (c) B15-3 ($\delta = 19$ mm) after impact.
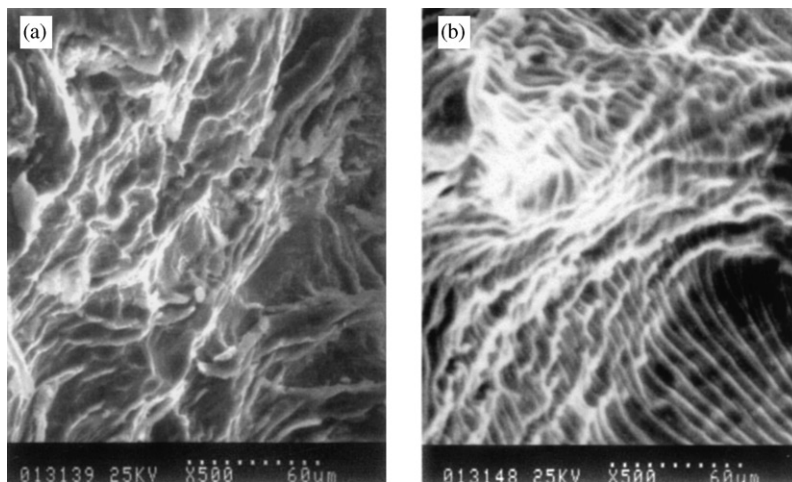

Fig. 20. SEM micrographs of fractured foam surface (a) of a quasi-statically loaded beam and (b) of a dynamically loaded beam.

ductile tensile profile, as shown in Fig. 20. Nevertheless, there is some difference between the two micrographs and the reason is not clear.

When a thin skin on a soft material is impacted, a wrinkle frequently occurs which will certainly reduce the load carrying capacity of the beam. Hence Mode I failure is unlikely to happen in dynamic tests.

4. Conclusions and discussion

The aluminum foam under investigation is strain-rate-insensitive within the strain range tested. It is shown that the deformation of aluminum foam specimens in dynamic compression is macroscopically uniform in the SHPB tests.

For the aluminum skin/aluminum-foam core sandwich beams, final failure occurs when the lower skin and the lower part of the core cracked due to tension. Quasi-static bending tests show two failure modes. In Mode I failure, no upper skin wrinkle occurs and the beam may carry a high load but is broken early. In Mode II failure, an upper skin wrinkle reduces the maximum load but the final deflection of the beam is larger than that in Mode I, leading to a higher energy absorbing capacity. Only Mode II failure was found in the dynamic bending tests due to local indentation by impact. The energy absorbing capacity of sandwich beams in dynamic cases was less than their quasi-static counterpart. The wrinkle, the local damage and the associated skin–core interface debonding are responsible for the degradation of the energy absorbing capacity.

Generally speaking, failure initiates from local damage. For a complex structure, different local damage mechanisms exist and the dominant one determines the final failure of a structure. In the cases of dynamic impact of sandwich beams, skin wrinkle is a phenomenon requiring more attention. As an unstable process, it is highly sensitive to many parameters. Hence it is more difficult to analyze. Among the parameters, mesoscopic inhomogeneity, as well as the shape of the loading head and the interface strength, plays an important role. Further theoretical analysis and experimental study are necessary before this failure mode is included in a failure map.

References

[1] Prakash O, Sang H, Embury JD. Structure and properties of Al–SiC foam. Mater Sci Eng 1995;A199:195–203.
[2] Beals JT, Thompson MS. Density gradient effects on aluminum foam compression behavior. J Mater Sci 1997;32:3595–600.
[3] Sugimura Y, Meyer J, He MY, Bart-Smith H, Grenstedt JL, Evans AG. On the mechanical performance of closed cell Al alloy foams. Acta Mater 1997;45(12):5245–59.
[4] Andrews E, Sanders W, Gibson LJ. Compressive and tensile behavior of aluminum foams. Mater Sci Eng 1999;A270:113–24.
[5] Gibson LJ, Ashby MF. Cellular solids: structure and properties. Oxford: Pergamon, 1997.
[6] Simone AE, Gibson LJ. Effects of solid distribution on the stiffness and strength of metallic foams. Acta Mater 1998;46(6):2139–50.
[7] Simone AE, Gibson LJ. The effects of cell face curvature and corrugations on the stiffness and strength of metallic foams. Acta Mater 1998;46(11):3929–35.
[8] Grenestedt JL, Bassinet F. Influence of cell wall thickness variations on elastic stiffness of closed-cell cellular solids. Int J Mech Sci 2000;42:1327–38.
[9] Lankford J, Dannemann KA. Strain rate effects in porous materials. In: Symposium Proceedings 521, Porous and Cellular Materials for Structure Applications, Warrendale: Materials Research Society, 1998, p. 103–8.

[10] Deshpande VS, Fleck NA. High strain rate compressive behaviour of aluminium alloy foams. Int J Impact Eng 2000;24:277–98.

[11] Mukai T, Kanahashi H, Miyoshi T, Mabuchi M, Nieh TG, Higashi K. Experimental study of energy absorption in a close-celled aluminum foam under dynamic loading. Scr Mater 1999;40(8):921–7.

[12] Mukai T, Kanahashi H, Yamada Y, Shimojima K, Mabuchi M, Nieh TG, Higashi K. Dynamic compressive behavior of an ultra-lightweight magnesium foam. Scr Mater 1999;41(4):365–71.

[13] Kanahashi H, Mukai T, Yamada Y, Shimojima K, Mabuchi M, Nieh TG, Higashi K. Dynamic compression of an ultra-low density aluminium foam. Mater Sci Eng 2000;A280(2):349–53.

[14] Paul A, Ramamurty U. Strain rate sensitivity of a closed aluminum foam. Mater Sci Eng 2000;A281(1):1–7.

[15] Chen C, Harte AM, Fleck NA. The plastic collapse of sandwich beams with a metallic foam core. Int J Mech Sci 2001;43:1483–506.

[16] Bart-Smith H, Hutchinson JW, Evans AG. Measurement and analysis of the structural performance of cellular metal sandwich construction. Int J Mech Sci 2001;43:1945–63.

[17] McCormack TM, Miller R, Kesler O, Gibson LJ. Failure of sandwich beams with metallic foam cores. Int J Solids Struct 2001;38:4901–20.

[18] Kesler O, Gibson LJ. Size effect in metallic foam core sandwich beams. Mater Sci Eng 2002;A326:228–34.

[19] Harte AM, Fleck NA, Ashby MF. The fatigue strength of sandwich beams with an alumimium alloy foam core. Int J Fatigue 2001;23:499–507.

[20] Harte AM, Fleck NA, Ashby MF. Sandwich panel design using aluminum alloy foam. Adv Eng Mater 2000;2(4):219–22.

[21] Hanssen AG, Langseth M, Hopperstad OS. Static and dynamic crushing of square aluminium extrusions with aluminium foam filler. Int J Impact Eng 2000;24:347–83.

[22] Hanssen AG, Langseth M, Hopperstad OS. Static and dynamic crushing of circular aluminium extrusions with aluminium foam filler. Int. J Impact Eng 2000;24:475–507.

[23] Santosa S, Wierzbicki T. Effect of an ultralight metal filler on the bending collapse behavior of thin-walled prismatic columns. Int J Mech Sci 1999;41(8):995–1019.

[24] Santosa S, Banhart J, Wierzbicki T. Bending crush resistance of partially foam-filled sections. Adv Eng Mater 2000;2(4):223–7.

[25] Hanssen AG, Hopperstad OS, Langseth M. Bending of square aluminium extrusions with aluminium foam filler. Acta Mech 2000;142(1–4):13–31.